Available online at www.sciencedirect.com

ScienceDirect

Current Opinion in Structural Biology

In situ structure determination by subtomogram averaging

Daniel Castaño-Díez[1] and Giulia Zanetti[2]

Cryo-tomography and subtomogram averaging are increasingly popular techniques for structural determination of macromolecular complexes *in situ*. They have the potential to achieve high-resolution views of native complexes, together with the details of their location relative to interacting molecules. The subtomogram averaging (StA) pipelines are well-established, with current developments aiming to optimise each step by reducing manual intervention and user decisions, following similar trends in single-particle approaches that have dramatically increased their popularity. Here, we review the main steps of typical StA workflows. We focus on considerations arising from the fact that the objects of study are embedded within unique crowded environments, and we emphasise those steps where careful decisions need to be made by the user.

Addresses
[1] BioEM Lab, Center for Cellular Imaging and Nanoanalytics, Biozentrum, University of Basel, Mattenstrasse 26, CH-4058, Basel, Switzerland
[2] Institute of Structural and Molecular Biology, Birkbeck College, Malet St., London, WC1E 7HX, UK

Corresponding authors:
Castaño-Díez, Daniel (daniel.castano@unibas.ch),
Zanetti, Giulia (g.zanetti@mail.cryst.bbk.ac.uk)

Current Opinion in Structural Biology 2019, **58**:68–75

This review comes from a themed issue on **Biophysical and computational methods**

Edited by **Laura Itzhaki** and **Alan Lowe**

https://doi.org/10.1016/j.sbi.2019.05.011

Introduction

Cryo-electron tomography is the technique of choice for structural analysis of biological complexes in their native context. Through imaging in the electron microscope at a range of tilt angles, a 3D reconstruction is obtained of pleiomorphic and unique specimens. If many copies of a complex of interest are present within the tomographic reconstruction, subtomogram averaging (StA) can significantly increase its resolution, without detracting from the advantage that the reconstructed objects are embedded within their native biological context. StA is increasingly used for structural analysis of protein complexes *in situ*, whether it be in eukaryotic cells (e.g. Nuclear pore complexes [1•,2], ribosomes [3], proteasomes [4,5], coat protein complexes [6•,7]) bacterial cells (e.g. secretion systems [8,9•,10], flagellar motors [11,12], S-layer [13]), in purified organelles or viruses (e.g. viral glycoproteins [14,15], viral capsids [16••,17], mitochondrial complexes [18–20], translating ribosomes [21]), or on reconstituted systems (e.g. membrane remodelling coat complexes [22••,23,24], cytoskeletal motors [25]).

The typical workflow of StA is represented in Figure 1. It starts with collection of a tilt series, and tomogram reconstruction, and then it involves particle picking, subvolume extraction and generation of a starting reference, upon which iterations of alignment and averaging, and eventually classification are performed. The structures that are obtained are subjected to postprocessing and validation before being interpreted. At many stages through the process, the results can inform the previous steps, which can be repeated with refined parameters.

Processing cryo-tomographic data has necessitated development of *ad hoc* protocols to deal with tilted images and with anisotropic 3D volumes [26,27]. For instance, defocus-dependent modulation of image frequencies (as defined by the Contrast Transfer Function, CTF) varies across tilted images and within the height of the reconstructed volume, requiring dedicated CTF correction software. The limited angular range to which samples can be tilted (typically ±60°) leads to anisotropy in the reconstructed volumes (described as a missing-wedge in Fourier space), which must be compensated during subvolume alignments [26,27]. Moreover, while the complexity and diversity of the samples analysed are usually the reasons why StA is chosen over single particle analysis or other structural techniques, it also implies that data analysis protocols must be adapted to the object of interest. This is especially true during particle picking, initial orientation assessment, and in the validation and interpretation stages, as outlined below.

Here, we review the typical steps of the StA workflow (Figure 1), with an emphasis on those aspects that must be optimised depending on the particular context of the object analysed.

Figure 1

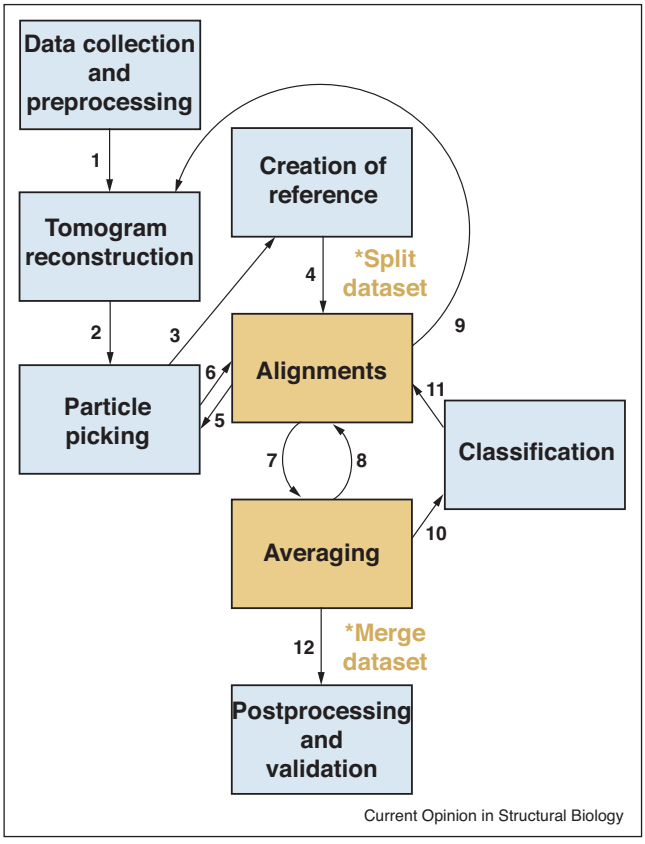

Overview of the typical subtomogram averaging workflow. 1. Upon data collection, images are subjected to frame alignment, dose compensation, and – in some protocols – CTF correction, then back-projected to reconstruct the tomogram. 2. Coordinates for particle picking are defined and subvolumes extracted. 3. These can be averaged to obtain a starting reference. 4. The reference is then used to align subvolumes. At this stage the data set should be split in halves to follow gold-standard procedures. 5, 6. The first alignments can provide refined coordinates for subvolume extraction. 7, 8. Alignments and averaging cycles are iterated until convergence. 9. In some protocols, subtomogram alignments can be used to refine the tilt geometry and obtain a more accurate tomogram reconstruction, from which higher resolution subtomograms can be extracted. 10, 11. During or after alignment, classification can be used to separate heterogeneous groups of particles. 12. The final averages are subjected to postprocessing (amplitude weighting and sharpening), and validation.

Preprocessing and tomogram reconstruction

When reconstructing cryo-tomograms for subtomogram averaging it is desirable to preserve high resolution information as much as possible. To this aim, pre-processing of tilt images includes steps that have been optimised for high-resolution single particle cryo-EM. Motion correction of frames within each tilt image improves on the degrading effects of beam induced sample motion and of drift. Drift tends to be worse at high tilts, making motion correction especially important in cryo-tomography. Exposure filtering to remove cumulative electron damage-derived noise [28] can be implemented on a tilt-by-tilt basis or within subframes of every tilt. Exposure filters work optimally when paired with dose-symmetric data collection schemes, where the high tilt images, in which high resolution information is corrupted by increased thickness and lower precision of CTF estimation, are effectively filtered in the dose-compensation procedure [29•].

To maximise high-resolutions in the averaged subtomograms, it is important that tilt images are aligned with the highest possible accuracy before back-projection. Tilt geometry must be optimised by iteratively minimising the residual differences between the actual positions of sample features and those predicted by the best geometrical tilt model [30,31]. When possible, this should be done using gold beads as fiducials. In certain samples (e.g. cell sections or lamellae), it is not possible to add gold beads and alignments must rely on image 'patches' to serve as fiducials [32,33]. Success in this case depends on the amount of signal available.

Currently, obtaining high-quality tilt series alignments suitable for high-resolution structure determination requires a manual procedure of fiducial optimisation, which significantly decreases the throughput. Recent developments use alignments of subtomograms to further refine the local geometry of the tilt series, improving high-resolution signal ([34], further discussed in the 'Alignment and averaging' section).

Accurate CTF estimation and correction are important aspects to consider when aiming to preserve high-resolution features. As discussed above, dose-symmetric tilt schemes ensure that the high resolution information is preserved in the lower tilts, where CTF estimation is more accurate due to higher SNR [29•]. Compared with single-particle reconstruction, cryo-tomography has the advantage that the relative defocus is known for each voxel in the reconstruction. This allows to calculate a 3D-CTF-corrected tomogram by back-projecting image pixels where signal has been restored using the appropriate z-height-adjusted defocus values [35,36•].

Tomogram content analysis

Current Single Particles Analysis studies handle the localisation of individual particles on micrographs as a straightforward task. In contrast, embarking on an StA project requires a decision on the specific strategy to determine the approximate locations of copies of the protein of interest inside each tomogram.

In the simplest scenario, particles can be selected as individual entities, both through manual inspection and interaction with the tomograms [37] or through some automated approach for pattern recognition. Such

approaches range from exhaustive testing of the tomogram searching local maxima of similarity to a given template measured by cross-correlation [38], to more sophisticated applications of deep learning [39,40], a technique of artificial intelligence where the software is trained to mimic the performance of an expert human operator.

However, the signature ability of tomography is the exposition of the molecular context. Frequently the spatial location of the particles of interest in a tomogram is related to an approximately identifiable geometric distribution, induced by an organised structure in the cellular milieu. Particles may be arranged as decorations, embedded insets, or building blocks of filamentous or membranous structures, with different levels of regularity. Particle identification in these cases can be articulated along the characterisation and modelling of the underlying shape (Figure 2). Parametrisation of – for example – a microtubule as a bent cylinder (Figure 2a), of a vesicle as an ellipsoid (Figure 2b) or of a mitochondrial membrane as a triangulated manifold (Figure 2c) allows to exploit the predicted spatial correlation of the particles in relation to such objects and extract them collectively. Hereby, the model is used to create a set of spatial locations, generated under the double constraint of being consistent with the support geometry and also within a physically meaningful distance among each other. For a sufficiently dense distribution of positions and a sufficiently large cropping side length, boxes extracted around these locations will probably contain actual particles, although the position of the particle inside the subtomogram box will be random. The positions of particles inside the boxes can then be estimated through alignment of subtomograms, a procedure that can be aided by the approximate orientation that can be inferred for each particle from its relation to the model (typical examples are the normal to a membrane, or the direction of the axis of a filament) (Figure 3a,b [22••,23]).

As an organised structure might contain a large number of particles (ranging between tens and hundreds depending on the particular case), computer tools for efficient on-screen annotation of support geometries are a powerful resource [37]. Complementarily, the identification of support geometries can be facilitated through volumetric segmentation methods [41], ideally tailored to the characteristic of cryoET data — mainly low SNR and the presence of missing wedge [42,43]. In this insight, recent studies have explored the suitability of deep learning approaches for semiautomated identification of some of the structures in the cellular environment that are typically used as supporting geometries for subtomogram extraction [39].

Alignment and averaging

StA seeks to reconstitute the 3D shape of a macromolecular compound by integrating the signal of multiple noisy

Figure 2

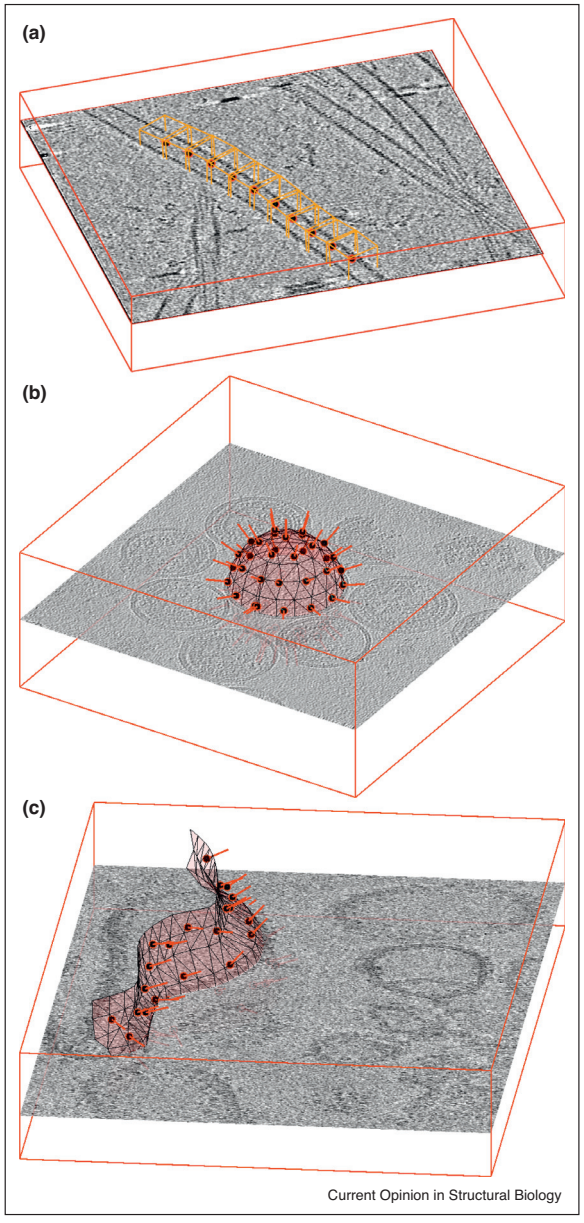

Examples of particle extraction for **(a)** filaments, **(b)** vesicles and **(c)** generically shaped membranes. In all three cases, the position of a subtomogram (red circle filled in black) is accompanied by an initial estimation of the orientation of the particle (red bar) given by the respective support geometry. In (a), orange boxes representing subtomograms are placed along the axis of a microtubule (data of microtubule-bound dynein–dynactin complexes from Grotjahn *et al.* [25]). The initial orientation of each subtomogram is given by the local orientation of the microtubule. In (b) the particles of interest are GAG proteins forming the capsid of HIV virus-like particles (VLPs) in solution (data from EMPIAR-10164). Their extraction is facilitated by using estimations of radius and centres to model the surface of the VLP as a sphere: locations of subtomograms are regularly distributed on it, while the local normals provide initial orientations. The tomogram in (c) shows membrane-assembled, *in vitro* reconstituted murine 5HT3 serotonins. The membrane of a non-spherical liposome is modelled as a triangulated surface, allowing the placement of a regular distribution of subtomogram centres and initial orientation assignations.

Figure 3

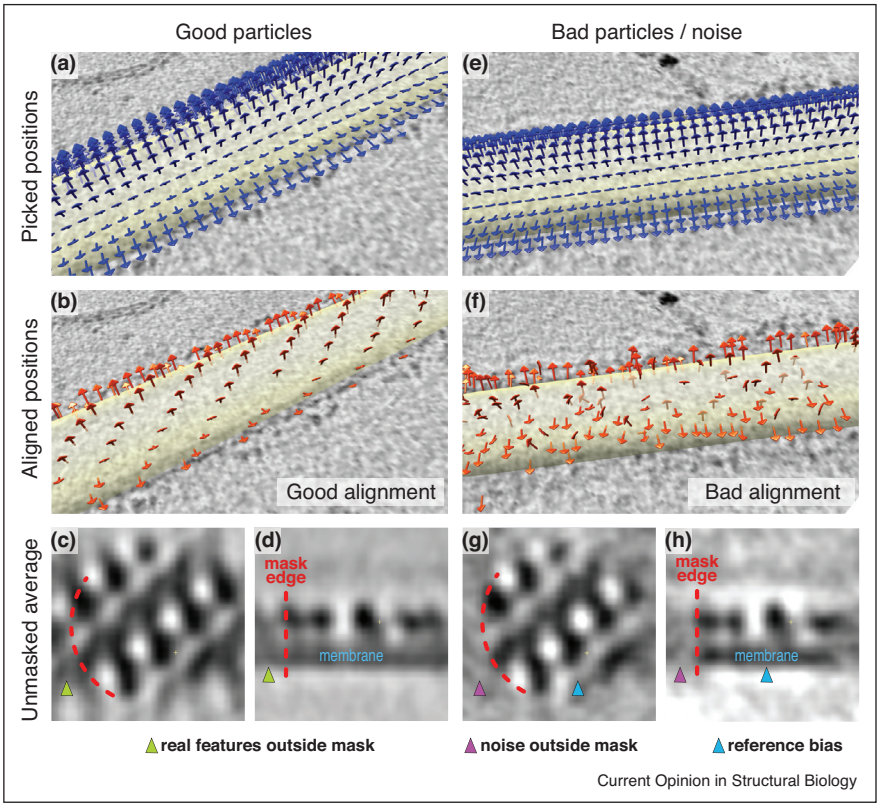

Example of validation in StA from COPII-coated tubules data [22••]. COPII forms a pseudo-helical lattice. **(a)** Arrows indicate the initial coordinates and orientations for particle picking on a coated tubule, where subvolume centres and sizes are chosen to oversample the tube surface, and rough orientations are assigned based on the underlying tubular geometry. **(b)** Coordinates after subtomogram alignment. The centres have shifted and form a clearly recognisable pseudo-helical pattern, validating the alignment. **(c,d)** Top and side cross-section of the average, respectively, obtained after alignments of subtomograms using a lattice-shaped starting reference and a mask (partially outlined in orange). The protein and membrane densities clearly continue outside the mask, validating the alignment. **(e–h)** As in (a–d), but on a tube where no ordered lattice was present. The pseudo-helical lattice is not apparent in (f), and in (g) and (h) the mask edge defines a sharp drop of the electron density, indicating that the average obtained mostly reflects reference bias.

copies contained in the extracted set of subtomograms. Knowledge of the exact orientation and location of each particle inside its subtomogram box allows to align all the particles to a common reference, then to average them coherently. StA finds these parameters in an iterative fashion. A density map used as initial reference is compared to each particle in the data set, locating the combination of translation and rotation that maximises the similarity of that particle to the reference. The alignment parameters of the entire data set are then used to create an average that will be used as reference for a new iteration until convergence is attained. This generic procedure is known as refinement and its implementation entails several practical considerations:

- The initial reference can be constructed by averaging a subset of the particles. In cases where the sample geometry allows to assign a rough initial orientation to particles (e.g. objects on a membrane or along filaments), the low-pass filtered reference created by averaging subtomograms will contain low-resolution features that correlate with those of each particle, greatly facilitating alignments. For example, the initial reference for particles extracted from the surface of a membrane might look like a smooth piece of membrane with relevant curvature.
- Frequently, the particle of interest does not appear as an isolated entity inside the subtomogram, but embedded into a high intensity structure (as a membrane or filament), or closely surrounded by other inhabitants of the cytosol. This calls for a careful masking of the initial reference, that is, providing the algorithm with a mask file that expresses which pixels in the reference should contain the particle – and thus common signal in all subtomograms – and which ones can vary its content among the data set.

- Similarity between reference and particle is measured through cross-correlation (refs), with appropriate adaption to account for the missing wedge of the tomogram and the mask imposed on the reference. Alternative approaches based on maximum likelihood use the similarity measured for each combination of translation of rotation to assign to it a probabilistic weight [44,45]. Either way, the best combination of translation and rotation parameters for a particle are determined by exhaustively testing on a set of shifts and Euler angles. Computationally, this calculation constitutes the most demanding task, and different approaches are available to reduce computing time: the set of scanned angles can be constrained to a neighbourhood of previously found alignment parameters; Fourier convolution allows to compute all translations simultaneously for a given orientation; similarly spherical harmonic transforms allow the simultaneous computation of all rotations for a given translation [46]; finally, the structure of the operation (which reuses the same data in a large number of computations) enables GPU implementations to yield impressive speedup factors [47].

Recent efforts explore the use of the alignment parameters computed on a set of subtomograms to realign the tilt series using the particles themselves as fiducials, refining the alignment generated by gold beads [34]. This potentially leads to more accurately aligned tilt series and correspondingly better tomograms and subtomograms, which, in turn, can be refined to produce a better alignment. This procedure can be iterated till convergence, and has been shown to produce considerable improvements for samples with large numbers of copies per tomogram.

Classification

Classification methods that have been reported to deal with heterogeneity can be separated into i) approaches aimed at characterising the heterogeneity of an *aligned* data set, and ii) algorithms performing classification and alignment simultaneously. In the former group, a frequent starting point is the exhaustive computation of the similarity of each pair of aligned subtomograms, giving rise to a covariance matrix. This matrix can be used to feed a Hierarchical Clustering method that locates groups of mutually similar particles [48], or as basis for a Principal Component Analysis [49], a widely used method for complexity reduction that captures the spatial features describing the largest sources of structural variance in the data set. Such features (eigen volumes) appear in order of relevance and can be used to express each particle as a reduced number of coefficients, which can then be clustered through k-means. Performance of these methods has been shown to improve significantly by a data-driven tuning of frequency band used to measure particle similarity [34].

The second family of methods is based on competitive alignment. The algorithm compares each particle with a set of different references, and assigns it to the reference that yields the highest score. As subsequent refinement iterations generate gradually better references, particle assignments can swap from one reference to other as the iterations progress. This procedure is similar to maximum-likelihood-based approaches which replace unique class assignments with probability weights [50].

In both families, masking constitutes a crucial decision, as it allows one to focus the analysis on the parts of the compound deemed to be flexible or conformationally different. While most methods allow to integrate this information as a prior if available, others are specifically designed to automatically analyse the regions of maximal variance to generate data-driven masks that update as the classification advances [51].

Validation

Once the classification and alignment procedures have reached convergence the final average is ready to be interpreted: subunits and domains are assigned and, where available, atomic models are fitted or built. Validation of the structure is crucial before any interpretation can be attempted. Many of the validation strategies in subtomogram averaging are shared with single particle reconstruction methods: for instance, the risk of creating an artefactual average through overfitting can be mitigated by the gold standard procedure [52]. This implies comparison between half datasets which were independently aligned against a band-pass filtered reference. Only information which is recovered beyond the high frequency limit of the reference filter can be considered for the next alignment iteration, and eventually defines the resolution to which the average can be interpreted.

Resolution is commonly assessed by Fourier Shell Correlation (FSC) [53]. The effects of using masks on the FSC have been described, and can be mitigated by phase randomisation methods [54]. Often, protein and lipid density within subtomograms continues beyond the actual particles to encompass associated macromolecules until the periphery of the box. The choice of mask will therefore significantly affect the average resolution, as non-correlating features are included in the FSC calculation. For this reason, and because of the inherent flexibility of all biological complexes, especially when resolved *in situ*, it is often desirable to measure the local resolution [55,56]. This might be combined with local filters to obtain a map where it is possible to interpret each feature at the appropriate level of detail. It remains important to calculate the gold-standard FSC as a diagnostic tool for overfitting or other typical artefacts [57••].

In cryo-tomography, the contextual information can be often used for validation of the alignments (as

exemplified in Figure 3). For example, when subunits are arranged in a pattern with respect to each other, and particle picking was performed by oversampling the underlying geometrical model (Figures 2 and 3a,e) then the convergence of neighbouring subtomograms to form a recognisable pattern is a very good validation of the correctness of the alignments (compare Figure 3b and f). Moreover, for embedded objects typical of StA, a mask applied during alignments may cut across continuous density, such as that of a membrane. In this case, correct alignment of 'real' particles will produce an average where the membrane is visible beyond the mask (Figure 3c,d), while incorrect alignments, or alignments of noise will produce an average where the density drops off suddenly outside the mask (Figure 3g,h).

Summary

The complexity of the biological samples typically analysed in cryo-tomography defines this technique and constitutes its biggest potential. At the same time, the reasons that make StA an attractive approach for structural determination also define its current limitations, for example, in relation to the inefficiency in attaining high numbers of particles, or to the bias in the alignments imposed by contextual information outside the 'particle' and the difficulty in defining optimal masks.

StA is currently relatively low-throughput with respect to cryo-EM single particle approaches. Nevertheless, there is scope for improvements in automation of StA pipelines, especially in data collection, pre-processing and tomographic reconstruction. StA will greatly benefit from comprehensive software packages to optimise each processing step without the need for continuous conversion between formats and conventions [34,58,59]. Software which will facilitate the flexible combination of different approaches will also significantly improve usability and help expand the user community—similarly to what has been implemented in single particle analysis [52,60].

So far, only a few StA projects have achieved near-atomic resolutions [16••,22••,34], but it is important to note that novel and insightful biological information can be retrieved from lower resolution studies, as long as appropriate validation procedures are implemented. This is especially true for cryo-tomography and StA, since the macromolecular structure itself only constitutes one aspect of the result: the information about the spatial relationship of the complexes of interest between each other, and with other neighbouring cellular features can often provide much precious insight into their function.

Conflict of interest statement

Nothing declared.

Acknowledgements

We would like to thank Joshua Hutchings, Himani Amin, Gabriel Lander and Danielle Grotjahn for sharing the data used in the figures. D.C.D. is supported by the Swiss National Science Foundation (SNF 205321_179041). G.Z. is supported by a Royal Society Dorothy Hodgkin Fellowship (DH130048), and an AMS Springboard award (SBF0031030).

References and recommended reading

Papers of particular interest, published within the period of review, have been highlighted as:

- • of special interest
- •• of outstanding interest

1. • Mosalaganti S, Kosinski J, Albert S, Schaffer M, Strenkert D, Salomé PA, Merchant SS, Plitzko JM, Baumeister W, Engel BD *et al.*: **In situ architecture of the algal nuclear pore complex**. *Nat Commun* 2018, **9**:2361.
The authors use cryo-FIB/SEM, cryo-tomography and subtomogram averaging to determine the structure of the NPC from Chlamydomonas cells.

2. Mahamid J, Pfeffer S, Schaffer M, Villa E, Danev R, Cuellar LK, Förster F, Hyman AA, Plitzko JM, Baumeister W: **Visualizing the molecular sociology at the HeLa cell nuclear periphery**. *Science* 2016, **351**:969-972.

3. Pfeffer S, Dudek J, Schaffer M, Ng BG, Albert S, Plitzko JM, Baumeister W, Zimmermann R, Freeze HH, Engel BD *et al.*: **Dissecting the molecular organization of the translocon-associated protein complex**. *Nat Commun* 2017, **8**:14516.

4. Albert S, Schaffer M, Beck F, Mosalaganti S, Asano S, Thomas HF, Plitzko JM, Beck M, Baumeister W, Engel BD: **Proteasomes tether to two distinct sites at the nuclear pore complex**. *Proc Natl Acad Sci U S A* 2017, **114**:13726-13731.

5. Guo Q, Lehmer C, Martínez-Sánchez A, Rudack T, Beck F, Hartmann H, Pérez-Berlanga M, Frottin F, Hipp MS, Hartl FU *et al.*: **In situ structure of neuronal C9orf72 Poly-GA aggregates reveals proteasome recruitment**. *Cell* 2018, **172**:696-705.e12.

6. • Bykov YS, Schaffer M, Dodonova SO, Albert S, Plitzko JM, Baumeister W, Engel BD, Briggs JA: **The structure of the COPI coat determined within the cell**. *eLife* 2017, **6**:e32493.
The authors use cryo-FIB/SEM, cryo-tomography and subtomogram averaging to determine the structure of the COPI complex from Chlamydomonas cells.

7. Kovtun O, Leneva N, Bykov YS, Ariotti N, Teasdale RD, Schaffer M, Engel BD, Owen DJ, Briggs JAG, Collins BM: **Structure of the membrane-assembled retromer coat determined by cryo-electron tomography**. *Nature* 2018, **561**:561-564.

8. Rapisarda C, Cherrak Y, Kooger R, Schmidt V, Pellarin R, Logger L, Cascales E, Pilhofer M, Durand E, Fronzes R: **In situ and high-resolution cryo-EM structure of a bacterial type VI secretion system membrane complex**. *EMBO J* 2019:e100886.

9. • Böck D, Medeiros JM, Tsao H-F, Penz T, Weiss GL, Aistleitner K, Horn M, Pilhofer M: **In situ architecture, function, and evolution of a contractile injection system**. *Science* 2017, **357**:713-717.
The authors use cryo-tomography and subtomogram averaging to determine the structure of the type 6 secretion system in bacterial cells.

10. Park D, Lara-Tejero M, Waxham MN, Li W, Hu B, Galán JE, Liu J: **Visualization of the type III secretion mediated Salmonella-host cell interface using cryo-electron tomography**. *eLife* 2018, **7**.

11. Kaplan M, Ghosal D, Subramanian P, Oikonomou CM, Kjaer A, Pirbadian S, Ortega DR, Briegel A, El-Naggar MY, Jensen GJ: **The presence and absence of periplasmic rings in bacterial flagellar motors correlates with stator type**. *eLife* 2019, **8**.

12. Qin Z, Tu J, Lin T, Norris SJ, Li C, Motaleb MA, Liu J: **Cryo-electron tomography of periplasmic flagella in *Borrelia burgdorferi* reveals a distinct cytoplasmic ATPase complex**. *PLoS Biol* 2018, **16**:e3000050.

13. Bharat TAM, Kureisaite-Ciziene D, Hardy GG, Yu EW, Devant JM, Hagen WJH, Brun YV, Briggs JAG, Löwe J: **Structure of the hexagonal surface layer on Caulobacter crescentus cells**. *Nat Microbiol* 2017, **2**:17059.

14. Tran EEH, Nelson EA, Bonagiri P, Simmons JA, Shoemaker CJ, Schmaljohn CS, Kobinger GP, Zeitlin L, Subramaniam S, White JM: **Mapping of ebolavirus neutralization by monoclonal antibodies in the ZMapp cocktail using cryo-electron tomography and studies of cellular entry**. *J Virol* 2016, **90**:7618-7627.

15. Riedel C, Vasishtan D, Siebert CA, Whittle C, Lehmann MJ, Mothes W, Grünewald K: **Native structure of a retroviral envelope protein and its conformational change upon interaction with the target cell**. *J Struct Biol* 2017, **197**:172-180.

16. •• Schur FKM, Obr M, Hagen WJH, Wan W, Jakobi AJ, Kirkpatrick JM, Sachse C, Kräusslich H-G, Briggs JAG: **An atomic model of HIV-1 capsid-SP1 reveals structures regulating assembly and maturation**. *Science* 2016, **353**:506-508.
Cryo-tomography and subtomogram averaging resolves the structure of the HIV capsid at near-atomic resolution.

17. Wan W, Kolesnikova L, Clarke M, Koehler A, Noda T, Becker S, Briggs JAG: **Structure and assembly of the Ebola virus nucleocapsid**. *Nature* 2017, **551**:394-397.

18. Davies KM, Anselmi C, Wittig I, Faraldo-Gómez JD, Kühlbrandt W: **Structure of the yeast F1Fo-ATP synthase dimer and its role in shaping the mitochondrial cristae**. *Proc Natl Acad Sci U S A* 2012, **109**:13602-13607.

19. Davies KM, Blum TB, Kühlbrandt W: **Conserved in situ arrangement of complex I and III2 in mitochondrial respiratory chain supercomplexes of mammals, yeast, and plants**. *Proc Natl Acad Sci U S A* 2018, **115**:3024-3029.

20. Pfeffer S, Woellhaf MW, Herrmann JM, Förster F: **Organization of the mitochondrial translation machinery studied *in situ* by cryoelectron tomography**. *Nat Commun* 2015, **6**:6019.

21. Pfeffer S, Burbaum L, Unverdorben P, Pech M, Chen Y, Zimmermann R, Beckmann R, Förster F: **Structure of the native Sec61 protein-conducting channel**. *Nat Commun* 2015, **6**:8403.

22. •• Hutchings J, Stancheva V, Miller EA, Zanetti G: **Subtomogram averaging of COPII assemblies reveals how coat organization dictates membrane shape**. *Nat Commun* 2018, **9**:4154.
Cryo-tomography and subtomogram averaging resolve the structure of the COPII coat assembled on membranes at 4.9 Å resolution.

23. Dodonova SO, Aderhold P, Kopp J, Ganeva I, Röhling S, Hagen WJH, Sinning I, Wieland F, Briggs JAG: **9Å structure of the COPI coat reveals that the Arf1 GTPase occupies two contrasting molecular environments**. *eLife* 2017, **6**.

24. Zanetti G, Prinz S, Daum S, Meister A, Schekman R, Bacia K, Briggs JAG: **The structure of the COPII transport-vesicle coat assembled on membranes**. *eLife* 2013, **2**:e00951.

25. Grotjahn DA, Chowdhury S, Xu Y, McKenney RJ, Schroer TA, Lander GC: **Cryo-electron tomography reveals that dynactin recruits a team of dyneins for processive motility**. *Nat Struct Mol Biol* 2018, **25**:203.

26. Wan W, Briggs JA: **Cryo-electron tomography and subtomogram averaging**. *Meth Enzymol* 2016, **579**:329-367.

27. Hutchings J, Zanetti G: **Fine details in complex environments: the power of cryo-electron tomography**. *Biochem Soc Trans* 2018, **46**:807-816.

28. Grant T, Grigorieff N: **Measuring the optimal exposure for single particle cryo-EM using a 2.6 Å reconstruction of rotavirus VP6**. *eLife* 2015, **4**:e06980.

29. • Hagen WJH, Wan W, Briggs JAG: **Implementation of a cryo-electron tomography tilt-scheme optimized for high resolution subtomogram averaging**. *J Struct Biol* 2017, **197**:191-198.
A dose symmetric tilt scheme is developed which has had a high impact on current data collection protocols for subtomogram averaging.

30. Kremer JR, Mastronarde DN, McIntosh JR: **Computer visualization of three-dimensional image data using IMOD**. *J Struct Biol* 1996, **116**:71-76.

31. Mastronarde DN, Held SR: **Automated tilt series alignment and tomographic reconstruction in IMOD**. *J Struct Biol* 2017, **197**:102-113.

32. Noble AJ, Stagg SM: **Automated batch fiducial-less tilt-series alignment in Appion using Protomo**. *J Struct Biol* 2015, **192**:270-278.

33. Castaño-Díez D, Scheffer M, Al-Amoudi A, Frangakis AS: **Alignator: a GPU powered software package for robust fiducial-less alignment of cryo tilt-series**. *J Struct Biol* 2010, **170**:117-126.

34. Himes BA, Zhang P: **emClarity: software for high-resolution cryo-electron tomography and subtomogram averaging**. *Nat Methods* 2018, **15**:955-961.

35. Kunz M, Frangakis AS: **Three-dimensional CTF correction improves the resolution of electron tomograms**. *J Struct Biol* 2017, **197**:114-122.

36. • Turoňová B, Schur FKM, Wan W, Briggs JAG: **Efficient 3D-CTF correction for cryo-electron tomography using NovaCTF improves subtomogram averaging resolution to 3.4Å**. *J Struct Biol* 2017, **199**:187-195.
A user-friendly software for 3D CTF correction that improves the resolution of subtomogram averaging.

37. Castaño-Díez D, Kudryashev M, Stahlberg H: **Dynamo catalogue: geometrical tools and data management for particle picking in subtomogram averaging of cryo-electron tomograms**. *J Struct Biol* 2017, **197**:135-144.

38. Frangakis AS, Böhm J, Förster F, Nickell S, Nicastro D, Typke D, Hegerl R, Baumeister W: **Identification of macromolecular complexes in cryoelectron tomograms of phantom cells**. *Proc Natl Acad Sci U S A* 2002, **99**:14153-14158.

39. Chen M, Dai W, Sun SY, Jonasch D, He CY, Schmid MF, Chiu W, Ludtke SJ: **Convolutional neural networks for automated annotation of cellular cryo-electron tomograms**. *Nat Methods* 2017, **14**:983-985.

40. Xu M, Chai X, Muthakana H, Liang X, Yang G, Zeev-Ben-Mordehai T, Xing EP: **Deep learning-based subdivision approach for large scale macromolecules structure recovery from electron cryo tomograms**. *Bioinformatics* 2017, **33**:i13-i22.

41. Pintilie G, Chiu W: **Comparison of segger and other methods for segmentation and rigid-body docking of molecular components in cryo-EM density maps**. *Biopolymers* 2012, **97**:742-760.

42. Martinez-Sanchez A, Garcia I, Asano S, Lucic V, Fernandez J-J: **Robust membrane detection based on tensor voting for electron tomography**. *J Struct Biol* 2014, **186**:49-61.

43. Luengo I, Darrow MC, Spink MC, Sun Y, Dai W, He CY, Chiu W, Pridmore T, Ashton AW, Duke EMH *et al.*: **SuRVoS: super-region volume segmentation workbench**. *J Struct Biol* 2017, **198**:43-53.

44. Scheres SHW, Melero R, Valle M, Carazo J-M: **Averaging of electron subtomograms and random conical tilt reconstructions through likelihood optimization**. *Structure* 2009, **17**:1563-1572.

45. Bharat TAM, Russo CJ, Löwe J, Passmore LA, Scheres SHW: **Advances in single-particle electron cryomicroscopy structure determination applied to sub-tomogram averaging**. *Structure* 2015, **23**:1743-1753.

46. Chen Y, Pfeffer S, Hrabe T, Schuller JM, Förster F: **Fast and accurate reference-free alignment of subtomograms**. *J Struct Biol* 2013, **182**:235-245.

47. Castaño-Díez D: **The dynamo package for tomography and subtomogram averaging: components for MATLAB, GPU computing and EC2 Amazon web services**. *Acta Crystallogr D Struct Biol* 2017, **73**:478-487.

48. Xu M, Beck M, Alber F: **High-throughput subtomogram alignment and classification by Fourier space constrained fast volumetric matching**. *J Struct Biol* 2012, **178**:152-164.

49. Förster F, Pruggnaller S, Seybert A, Frangakis AS: **Classification of cryo-electron sub-tomograms using constrained correlation**. *J Struct Biol* 2008, **161**:276-286.

50. Stölken M, Beck F, Haller T, Hegerl R, Gutsche I, Carazo J-M, Baumeister W, Scheres SHW, Nickell S: **Maximum likelihood**

based classification of electron tomographic data. *J Struct Biol* 2011, **173**:77-85.

51. Chen Y, Pfeffer S, Fernández JJ, Sorzano COS, Förster F: **Autofocused 3D classification of cryoelectron subtomograms**. *Structure* 2014, **22**:1528-1537.

52. Scheres SHW: **RELION: implementation of a Bayesian approach to cryo-EM structure determination**. *J Struct Biol* 2012, **180**:519-530.

53. van Heel M, Schatz M: **Fourier shell correlation threshold criteria**. *J Struct Biol* 2005, **151**:250-262.

54. Chen S, McMullan G, Faruqi AR, Murshudov GN, Short JM, Scheres SHW, Henderson R: **High-resolution noise substitution to measure overfitting and validate resolution in 3D structure determination by single particle electron cryomicroscopy**. *Ultramicroscopy* 2013, **135**:24-35.

55. Cardone G, Heymann JB, Steven AC: **One number does not fit all: mapping local variations in resolution in cryo-EM reconstructions**. *J Struct Biol* 2013, **184**:226-236.

56. Kucukelbir A, Sigworth FJ, Tagare HD: **Quantifying the local resolution of cryo-EM density maps**. *Nat Methods* 2014, **11**:63-65.

57. •• Penczek PA: **Resolution measures in molecular electron microscopy**. *Meth Enzymol* 2010, **482**:73-100.
A comprehensive and user-friendly software for subtomogram averaging and classification. Current versions of this package include tools for tilt series alignment, tomogram reconstruction and inspection, and particle picking.

58. Castaño-Díez D, Kudryashev M, Arheit M, Stahlberg H: **Dynamo: a flexible, user-friendly development tool for subtomogram averaging of cryo-EM data in high-performance computing environments**. *J Struct Biol* 2012, **178**:139-151.

59. Navarro PP, Stahlberg H, Castaño-Díez D: **Protocols for subtomogram averaging of membrane proteins in the dynamo software package**. *Front Mol Biosci* 2018, **5**:82.

60. de la Rosa-Trevín JM, Quintana A, Del Cano L, Zaldívar A, Foche I, Gutiérrez J, Gómez-Blanco J, Burguet-Castell J, Cuenca-Alba J, Abrishami V *et al.*: **Scipion: a software framework toward integration, reproducibility and validation in 3D electron microscopy**. *J Struct Biol* 2016, **195**:93-99.